



Science Arts & Métiers (SAM)

is an open access repository that collects the work of Arts et Métiers Institute of Technology researchers and makes it freely available over the web where possible.

This is an author-deposited version published in: <https://sam.ensam.eu>
Handle ID: <http://hdl.handle.net/10985/20498>

To cite this version :

Laurent PELTIER, Olivier PERROUD, Patrick MOLL, Jérôme SLOWENSKY, Pierre CHARBONNIER, André EBERHARDT, A. HAUTCOEUR - Production and Mechanical Properties of Cu-Al-Ni-Be Shape Memory Alloy Thin Ribbons Using a Cold Co-Rolled Process - Shape Memory and Superelasticity - 2021

Any correspondence concerning this service should be sent to the repository

Administrator : scienceouverte@ensam.eu



Production and Mechanical Properties of Cu-Al-Ni-Be Shape Memory Alloy Thin Ribbons Using a Cold Co-Rolled Process

L. Peltier¹ · O. Perroud² · P. Moll² · J. Slowensky² · P. Charbonnier² · A. Eberhardt³ · A. Hautcoeur³

Abstract The use of shape memory alloys for micro-actuators constitutes a field of application in which copper-aluminum-based alloys find their usefulness because they can reach higher activation temperatures and are easier to produce than titanium-based alloys, particularly by the method proposed in this work. SMA tapes are a two-dimensional structure that offers many design options such as stamping, punching, and deep drawing, but they are also suitable for laser cutting, engraving, stamping, and EDM machining. This work has been made to study the manufacture of copper-based shape memory alloys (SMAs) using the cold co-rolling process also called the cold-roll bonding (CRB) process. In this process, a thin metal sandwich can be produced with a rolling machine. This sandwich consists of layers of CuNiBe master alloy and Al. During the rolling phase, the sandwich has no shape memory effect (SME) or superelastic effect (SE), so thin strips can be easily produced. After the rolling phase, the sandwich is subjected to a complex heat treatment to gain the SME. To validate this process to produce Cu-based SMAs, several alloys with different CuAlNiBe compositions have been tested. The SMAs obtained were characterized by optical microscopy, scanning electron

microscopy (SEM) and X-ray diffraction (XRD) techniques. The martensitic transformation was studied by Differential Scanning Calorimetry (DSC) and SME and SE were studied by three-point bending tests. This work shows that the CRB is a good process for making a wide variety of Cu-based SMA ribbons.

Keywords Thin ribbon · Shape memory alloy · Superelasticity and shape memory behavior · Martensitic transformation · Cold-roll bonding process

Introduction

The shape memory alloys (SMAs) are SMART materials. They can respond to temperature changes by producing a visible deformation [1]. There are several families of SMAs: Cu-based alloys (CuZnAl, CuAlNi, CuAlMn, CuAlBe), NiTi-based alloys (NiTi, NiTiCu, NiTiNb), TiNb-based alloys (TiNb, TiNbZr, TiNbZrTa) and Fe-based alloys (FePt, FePd, FeNiCo, FeMnSi, FeMnAl). These materials are produced out using different processes, such as induction melting [2], arc melting [3], powder metallurgy [4], rapid solidification, mechanical alloying [5] and additive manufacturing [6, 7]. Cu-based SMA has been promising material because of its low price and its easier manufacturing process as compared to the Ti-based SMAs. CuAlNi alloys have been selected as high potential materials for high temperature applications (HT-SMAs). This is attributed to their high thermal stability at a temperature above 100 °C [8, 9]. However, these alloys have limitations such as the high brittleness, because of the appearance of γ_2 -phase at the grain boundaries [10] and the increase of the grain size during heat treatment [11]. Thus, their disadvantages have restricted the use of these alloys

✉ L. Peltier
laurent.peltier@ensam.eu

¹ Arts Et Métiers Institute of Technology, Université de Lorraine, CNRS, LEM3-UMR 7239, HESAM Université, 4, rue Augustin Fresnel, 57070 Metz, France

² Université de Lorraine, CNRS, Arts Et Métiers Institute of Technology, LEM3-UMR 7239, 7, rue Augustin Fresnel, 57070 Metz, France

³ Nimesis Technology, 4, Rue des Artisans Frontigny, 57245 Mécleuves, France

for commercial applications in particular in SE applications. One way to solve these problems is to refine the grain of the CuAlNi SMAs by adding some alloying elements such as Be or by varying the compositions of Ni and Al [12–14]. These changes have shown some improvement in mechanical properties. Xu et al. [15] shows that the fatigue life of a ternary CuAlNi alloy has been increased by adding Be. Zhu et al. [16] shows that the bending performances (σ_f and ϵ_f) of CuAlNiBe are higher than CuAlNi basic alloy. Therefore, the mechanical property of Cu-based SMAs can be significantly improved by adding alloying elements. In this work, the SMAs ribbons are produced by a cold co-rolled process also known as the cold-roll bonding (CRB) process or additive-roll bonding (ARB) process. The multilayer sandwich of master alloy and pure ductile aluminum is assembled and transformed into a thin ribbon of CuAlNiBe SMA by thermomechanical treatments. This particular CRB technique allows the sandwich to be rolled until the final thickness before it becomes a SMA. This technique allows choosing the property of the SMA according to the thickness of the Al layer during the cold welding of the sandwich.

Experimental methods

This work focuses on the characterization of the properties of a quaternary CuAlNiBe alloy. The compositions and thermal heat treatments are based on the studies of the phase diagrams and diffractograms of ternary CuAlNi and CuAlBe alloys. Although the Be element is very difficult to detect, especially when it is alloyed in very small quantities in the alloy and its amount is low enough to neglect it in using the phase diagrams, it is very important in determining the temperatures of the transformation points of the finalized alloy. The alloys studied in this work have compositions close to the eutectoid ternary phase diagram CuNiAl with 2 wt.% Ni [8, 9]. A relevant aspect of this work is the use of a master alloy CuNi_{1.9}Be_{0.4} which has been cast by the Trefimétaux company (wt.%). This composition is extracted from the isothermal section of the ternary diagram of CuAlNi at 800 °C for an alloy composition comprising between 1.1 and 1.6 wt.% Ni and between 10 and 14 wt.% Al (Fig. 1a). The Al used in this study was a commercial pure metal sheet. The strips were cold rolled to the chosen thicknesses: 0.4 mm for CuNiBe

Fig. 1 CuAlNi ternary phase diagrams; **a** isothermal section at 800 °C, **b** pseudo-binary phase diagram at 2 wt.% Ni

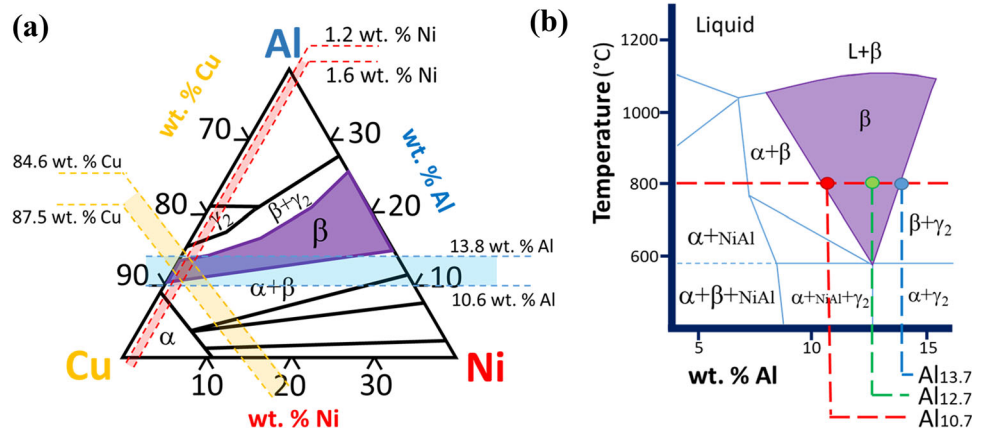
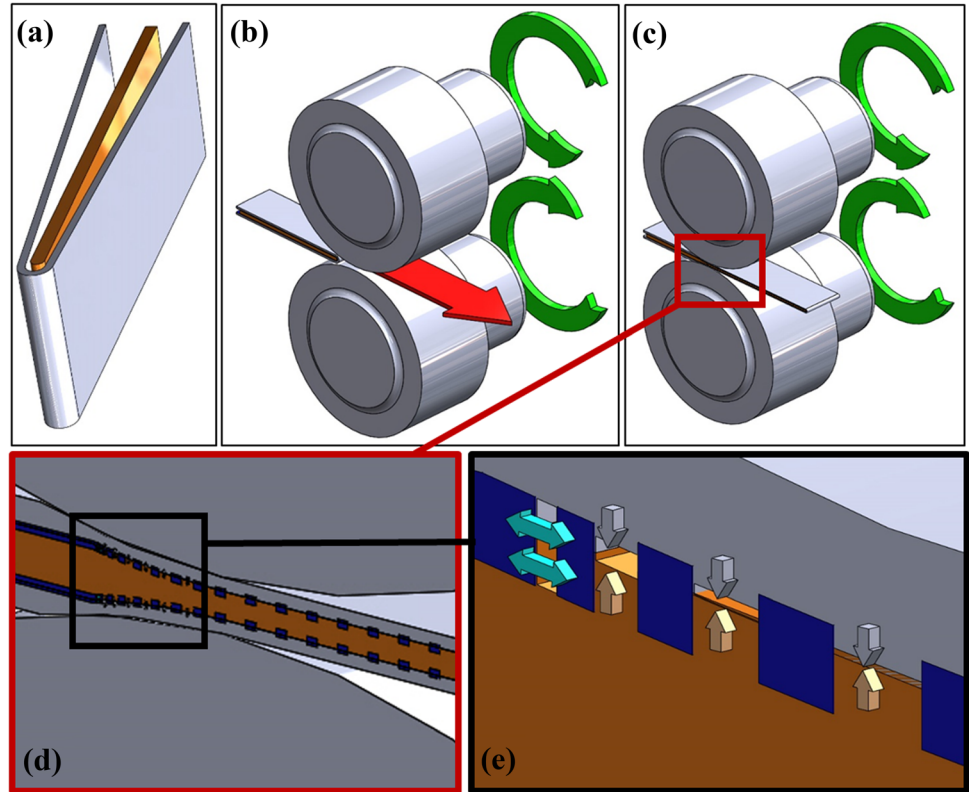


Table 1 Selected compositions of the three alloys (CuNiBe)_{100-x}Al_x: $x = 10.7$ for Al_{10.7} alloy, $x = 12.7$ for Al_{12.7} alloy, $x = 13.7$ for Al_{13.7} alloy (wt.%)

Layer thickness (mm)		Element (wt.%)				Calculated Ms (°C)	Designation
CuNiBe	Al	Cu	Ni	Be	Al		
0.4	0.070	88.27	1.64	0.370	9.72	227	Al10.7
0.4	0.075	87.82	1.59	0.365	10.22	193	
0.4	0.080	87.37	1.54	0.360	10.73	161	
0.4	0.085	86.92	1.49	0.355	11.23	130	
0.4	0.090	86.47	1.44	0.350	11.74	99	
0.4	0.095	86.02	1.39	0.345	12.24	68	
0.4	0.100	85.57	1.34	0.340	12.75	36	Al12.7
0.4	0.105	85.12	1.39	0.335	13.25	5	
0.4	0.110	84.67	1.24	0.330	13.76	- 26	Al13.7
0.4	0.115	84.22	1.19	0.325	14.26	- 58	
0.4	0.120	83.77	1.14	0.320	14.77	- 89	

Fig. 2 Schematic illustration of the cold rolling process; **a** metal sandwich composed of only two components, **b** and **c** the first cold rolling pass, **d** and **e** welding mechanism during the process: the horizontal arrows show the separation of the hardened layer, the vertical arrows show the extrusion of healthy material



master alloy and between 0.1 and 0.07 mm for Al (Table 1). At the beginning of this work, the state of the material is called as-received (AR).

Determination of the Chemical Composition of the SMAs Ribbons

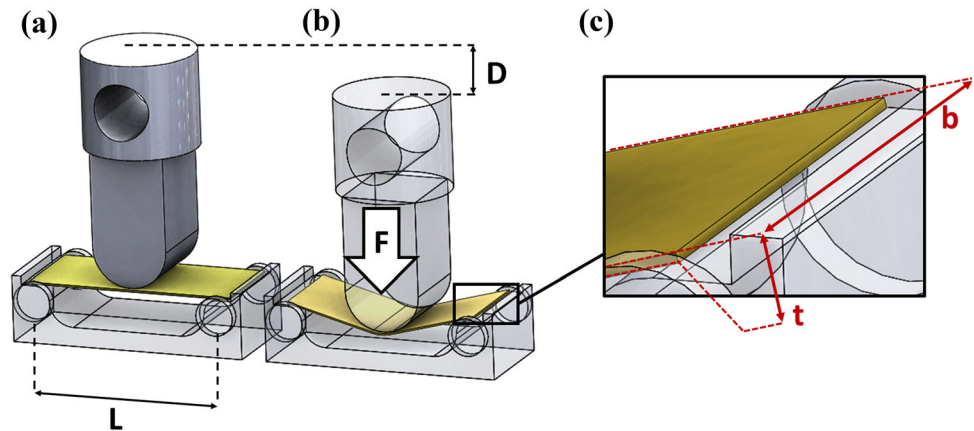
The elements and the concentration of the elements in the alloy composition affect the temperatures of the four transformation points in the SMAs. These points are respectively named Austenite Start (A_s), Austenite Finish (A_f), Martensite Start (M_s) and Martensite Finish (M_f). For example, the effect of Al content is much stronger than that of Ni, Mn, or Zn, but less than that of Be in Cu-based SMAs [17–19]. For Belkahla et al. the influence of Be is twelve times greater than that of Al. In the other studies cited, the influence of Al is on average eight times greater than that of Ni. In this study, the temperature of M_s will be calculated from the equation proposed by Belkahla et al. [20] for CuAlBe ternary alloy and this equation will be corrected if necessary by adding the adequate coefficient of Ni wt.% after the DSC tests of the manufactured alloys. The acceptable limits for the Al wt.% are given by the CuAlNi pseudo-binary diagram with 2 wt.% Ni (Fig. 1b). In this work, increasing the concentration of Al content decreases the transformation temperatures M_s . The objective of the present work is to investigate the effect of Al

strip thickness on the transformation temperatures, the thermodynamic parameters and the microstructures of CuAlNiBe SMAs. Table 1 shows the compositions of three alloys studied in this work (respectively named Al_{10.7} alloy, Al_{11.7} alloy and Al_{13.7} alloy) and resulting from the evolution of Al thickness in the initial sandwich (before homogenization heat treatments).

Cold Welding of the Sandwich

The SMAs thin ribbons are usually produced by melt spinning [8, 21, 22]. This technique does not allow the choice of the thickness and width of the finished product. In this work, welding by rolling allows choosing the final thickness of the multilayer strip without superelastic effect (SE) or shape memory effect (SME) behaviors before it is transformed into SMA by heat treatments. The mechanisms producing metallic bonds in cold welding were studied by Bay et al. in the 1980s [23, 24]. CRB [25] and ARB processes [26] are widely used to obtain binary, ternary or quaternary SMAs: CuZnAl [27, 28], CuAlMn [29, 30], CuAlNi, CuAlBe and Niti [31, 32]. In the present work, the metal sandwich is composed of a middle plate of CuNiBe which is placed between the folded Al plate (Fig. 2a). To deform all the different layers of the sandwich in the same way during the first cold co-rolling pass, the master alloy is fully annealed with a heat treatment under pure argon gas

Fig. 3 Three-point bending set-up: **a** unloading configuration, **b** loading configuration, **c** details of the SMA ribbon



(500 °C/1 h/No quench), the aluminum remains cold worked. After, both plates are prepared by the surface hardening process. For the middle plate of CuNiBe alloy, the process is carried out on both surfaces whereas, for the outer plate, it is carried out on the inner surface. For the hardening process, the sheets are polished, wire-brushed and then rinsed with acetone and alcohol for degreasing. To finish the hardening process, the plates are placed in a furnace at 200 °C for 30 min with a controlled atmosphere (with a gas mixture of argon at 80% and oxygen at 20%) to develop thin and fragile oxide layers. Figure 2 illustrates the principle of the cold co-rolling process. The different plates were stacked together (Fig. 2a), assembled and welded by cold co-rolling deformation. The sandwich is co-rolled to 60% reduction in thickness during the first pass (Fig. 2c). During this first rolling phase (Fig. 2b, c), the hardened layers between Al and CuNiBe break (the blue horizontal layer and blue arrows in Fig. 2d, e). Between the hardened aggregates, the healthy and pure material is extruded on both sides of the components of the sandwich (the grey and orange vertical arrows in Fig. 2d, e). Jamaati et al. [25] review the main technique and science involved in the cold-roll bonding (CRB) process. Jamaati et al. propose a mapping of the material combinations that can be bonded by cold welding. This mapping takes account the lattice structure and the hardness of the metal at room temperature. Thus, the elements Cu, Ni and Al are compatible to each other and are good candidates for the CRB process. The Be element is only compatible with the Cu element, but in the case of the master alloy used in this work, the Be element is pre-alloyed and will not hinder with the welding of the different layers of the sandwich. As a result, there is a cold-welding process when Al and CuNiBe alloy come into contact (Fig. 2e). This cold-welding process is reinforced by continuous crushing during rolling during the numerous rolling passes necessary to obtain the required thickness for the study.

Heat Treatment of the Sandwich

After the rolling steps, the sandwich undergoes a complex heat treatment that begins with a slow interdiffusion of the Al-CuNiBe system at 550 °C for several hours (Fig. 4a) [33]. The heat treatment consists of several steps including isothermal segments: 550 °C below the melting temperature (T_m) of Al, 670 °C just above the T_m of Al, 800 °C to reach the β -phase (Fig. 1b). After this heat treatment of homogenization, the alloys are solution treated (ST state) with quenching to obtain martensite, strictly necessary for the development of SME. This process is done using a custom quenching set-up to preserve the flatness of thin ribbons. This apparatus consists of two articulated water-cooled thick copper plates. During the first step of the heat treatment, there is interdiffusion between CuNiBe master alloy and Al. The bright appearance of the aluminum band, on the surface of the sandwich, gradually disappears showing that the different elements begin to mix in a solid-state diffusion bond (SSD). It was assumed that Al will first diffuse into the master alloy especially at 550 °C [33]. During this step of the heat treatment, a thin yellow layer forms between aluminum (anthracite grey color) and mother alloy (copper color). This thin yellow layer is the premise of the future CuAlNiBe alloy. The last step of the heat treatment (800 °C) insures the complete diffusion of Al in the matrix [34, 35] and finally the obtaining the β -phase (Fig. 1b) which represents the parent phase for further martensitic transformations, necessary to experience shape memory behaviors [17, 18].

Characterization of the Phase Transformation

The martensitic transformation of the ribbons is analyzed by differential scanning calorimetry (Setaram DSC 131). The tests are performed with a cooling and heating rate of 10 K/min over the temperature range (– 100–250 °C) on samples of 40 mg (ASTM standard F2004-17) [36]. The

thermograms from the DSC studies of the various alloys are post-processed using a dedicated software able of determining the four transformation temperatures characterizing an SMA: Austenite Start (A_s), Austenite Finish (A_f), Martensite Start (M_s) and Martensite Finish (M_f). The microstructural study of the co-rolled samples is characterized using optical microscope Zeiss AX10 and Nomarski differential interference contrast to observe the martensite phase. The local chemical composition of the samples, especially in the interdiffusion area between Al and CuNiBe alloy layers, are analyzed by energy-dispersive X-ray (EDX) with a Zeiss Supra 40 scanning electron microscopy (SEM). The crystallographic phases are analyzed by Rigaku X-ray diffraction using Cu-K α radiation at room temperature (T_R) after each step of the diffusion treatment (XRD powder mode, accelerating voltage of 40 kV and an intensity of 30 mA).

Characterization of the Superelasticity

The superelastic behavior of SMA ribbons is determined by low cycling fatigue tests with a three-point bending bench (Fig. 3a, b) according to the ASTM F2082 [37]. The test bench is designed to determine the flexural stress/strain curve of an SMA ribbon in the austenite phase on a large range of temperatures (25–250 °C). These tests have been carried out on a tension/compression universal machine

Zwick equipped with a thermal chamber. The diameter of the central loader support is 8 mm and limits the maximum flexural strain to 2.5%. The bending tests have been achieved at a displacement rate (crosshead speed) of 2 mm/min. Due to the large range of temperature, it was not possible to use a contact extensometer. As the deformation of the machine due to its compliance is compensated (the resolution of the displacement of the crosshead given by the manufacturer is of the order of the micrometer), the deflection has been calculated from the crosshead displacement recorded in real-time using the control software (TestXpert). This software automatically calculates flexural stress (σ_f) and flexural strain (ϵ_f). The data required for the calculation are the width (b) and the thickness (t) of the ribbon and the distance between supports (L). During the test, the machine registers the displacement (D) of the crossbar and the flexural load (F) necessary to obtain this displacement. σ_f and ϵ_f are calculated by the Euler–Bernoulli beam theory:

$$\epsilon_f = \frac{6Dt}{L^2} \quad \text{and} \quad \sigma_f = \frac{3FL}{2bt^2}$$

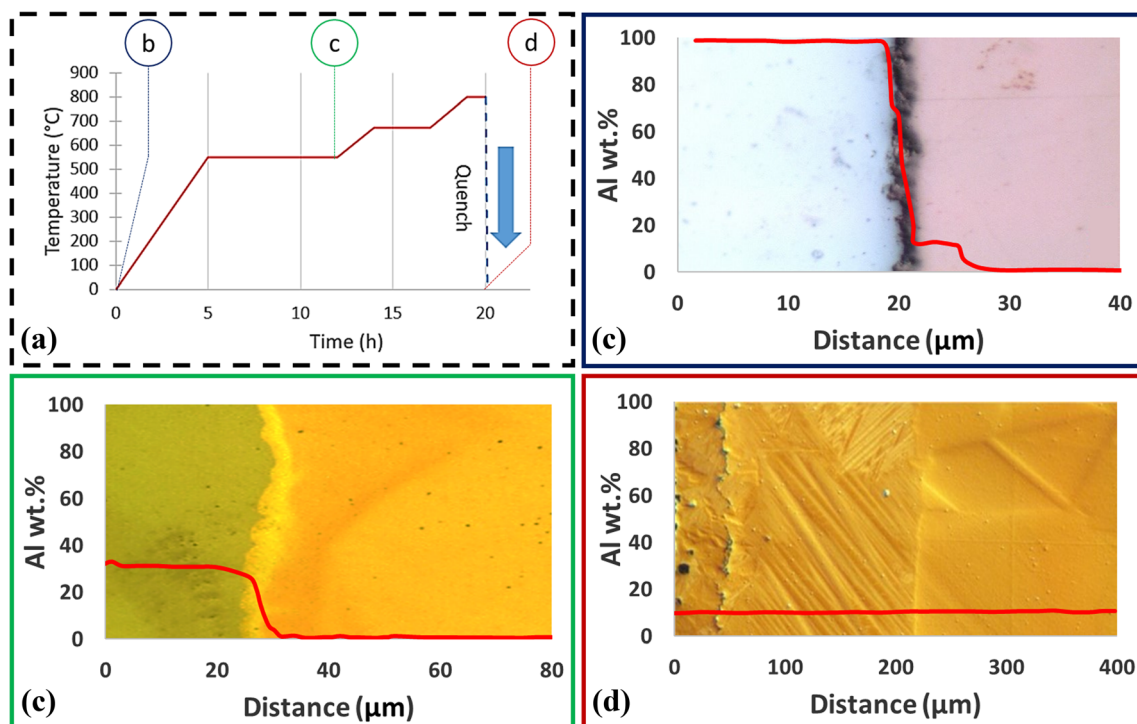


Fig. 4 Evolution of microstructure and chemical composition in the interphase boundary region of the Al12.7 alloy in the different diffusion steps involved in the formation of SMA ribbons; **a** schematic representation of the heat treatment, **b** cold welding step, **c** SSD step, **d** ST state

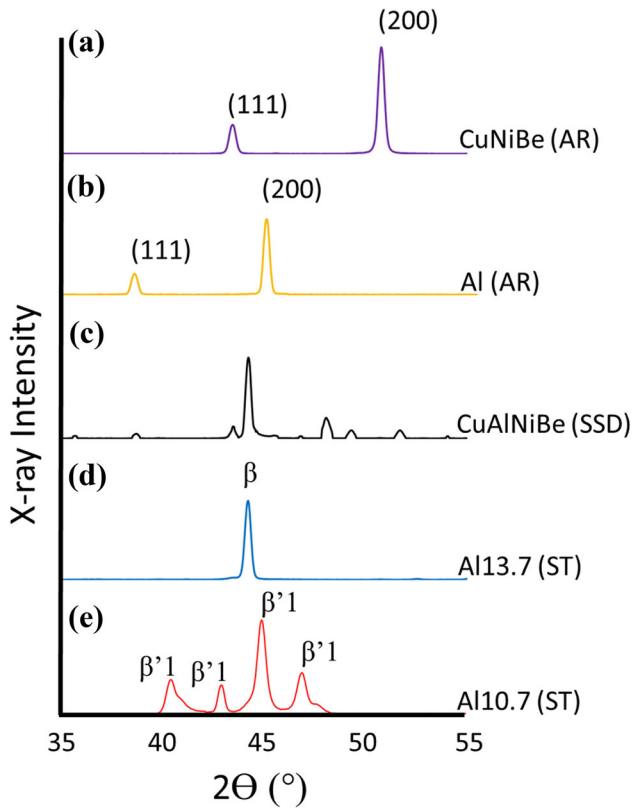


Fig. 5 X-ray diffractograms; **a** CuNiBe0.4 master alloy in AR state, **b** pure Al in AR state, **c** Al13.7 alloy after 5 h at 550 °C in SSD state. After quench; **d** Al13.7 alloy in austenitic phase at TR and **e** Al10.7 alloy in martensitic phase at TR

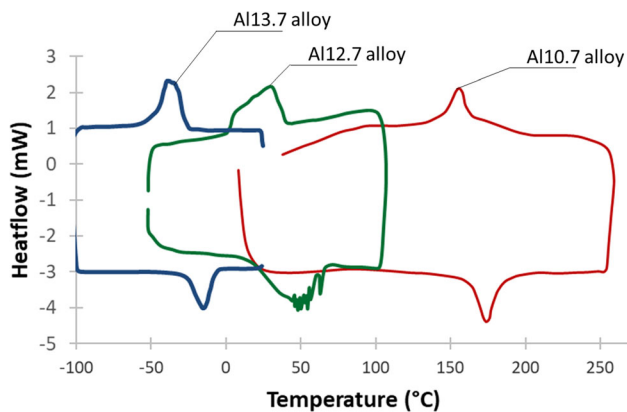


Fig. 6 DSC thermogram analysis of three nominal compositions of Al_{13.7}, Al_{12.7} and Al_{10.7} alloys

Experimental Results

Figure 4b, c and d show optical micrographs of the cross-section of the sample of the Al_{12.7} alloy in various states of the diffusion and homogenization processes. Before the heat treatment, the layers composing the sandwich are distinguished in Fig. 4b. One of both bonding interfaces between the sheets appeared as a dark grey line in Fig. 4b.

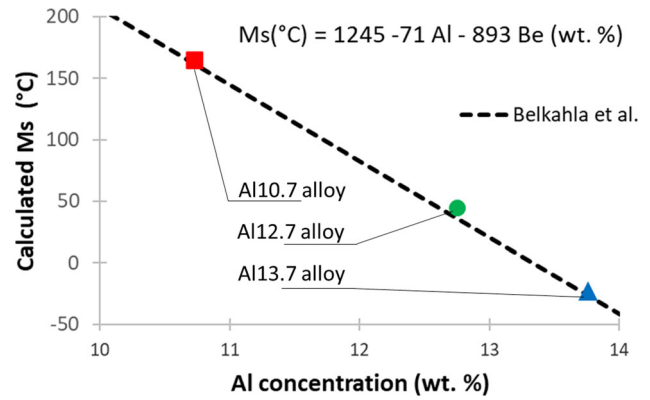


Fig. 7 Measured M_s temperature for the compositions of Al_{13.7}, Al_{12.7} and Al_{10.7} alloys compared to calculated M_s temperature as a function of Belkahla equation

The chemical analyses, in Fig. 4b, show that pure Al and CuNiBe alloy came into contact to create a good bonding during cold co-rolling. Sometimes the bonding does not work that creates voids. These voids are due to the oxidation hardened layer or impurities that the cleaning has not removed. Kirkendall shows that when two distinct materials are placed next to each other, a diffusion is allowed to take place between them [38]. After the heat treatment, the voids are more numerous (Fig. 4d) [29, 31, 34]. By Fick's 1st law of diffusion, the diffusion coefficients of the different alloys or pure metals into each other are not the same and the flux of atoms from the material with the higher diffusion coefficient will be larger. This phenomenon is only possible if diffusion occurs by an exchange mechanism [34]. An important consideration from the Kirkendall effect is the presence of voids formed during the diffusion process [39]. These porosities occur due to the difference in the diffusion rate of the two alloy species in an attempt to restore equilibrium.

The thermoelastic martensitic transformation is the origin of the SME and occurs in the Cu-based SMAs starting from the ordered cubic phase β . This study focuses on determining the possibility of obtaining the β -phase of the CuAlNiBe prepared by co-rolling and comparing the XRD results with the earliest studies devoted to more conventional alloy production methods [22, 40–43]. Figure 5 shows the X-ray diffractograms at T_R for different steps of the manufacturing process. Figure 5a shows the diffractogram of the CuNiBe master alloy used in this work, Fig. 5b shows that of pure Al. Figure 5d and e show respectively the alloys Al_{10.7} alloy in the austenitic state and Al_{13.7} alloy in the martensitic state (at T_R after heat treatment and water quench). The diffractogram in Fig. 5e also can be compared to the work of Zhu et al. [16] on a CuAl_{11.5}Ni_{4.5}Be_{0.4} (wt. %) alloy close to Al_{10.7} alloy. The XRD peaks of the two works are similar but not identical

because Zhu et al. proposes the study of a single crystal alloy. Figure 5c shows the diffractogram of Al_{10.7} alloy in SSD state after the heat treatment at 550 °C. This diffractogram shows many peaks suggesting a multi-phase alloy. In this diffractogram, there are the peaks of the Al, the peaks of CuNi [14, 44], the peaks of NiAl [45, 46] and those of the austenite phase of the Cu-based SMAs [47, 48].

Figure 6 shows the curves from the DSC studies of the three alloys Al_{13.7}, Al_{12.7} and Al_{10.7}. It shows that increasing the thickness of the aluminum layer in the sandwich augments Al amount in the alloy which decreases the temperature of the transformation points. Figure 7 shows the evolution of the temperature M_s as a function of wt.% Al and wt.% Be. Although Belkahlia et al. studied a CuAlBe ternary alloy without Ni, and so their fitting equation of M_s variation with Al content does not consider the wt.% Ni, the M_s values of Al_{13.7} alloy, Al_{12.7} alloy and Al_{10.7} alloy, derived from DSC thermograms, show a good correlation with Belkahlia equation.

The experimental analysis of the three alloys Al_{10.7}, Al_{12.7} and Al_{13.7} is completed by comparing their isothermal quasi-static fatigue responses during low cycling bending tests at the service temperature T_s (°C) = Af + 50 [respectively T_s (Al_{13.7}) = 50 °C, T_s (Al_{12.7}) = 120 °C, T_s (Al_{10.7}) = 240 °C]. Figure 8a relates a bending cycle (loading–unloading) that has been performed on the ribbons. Figure 8b, c and d present the loading flexural stress/

strain curves for different cycle numbers (C1, C50, C100) for the three alloys considered in the ST state. For the Al_{13.7} alloy at 50 °C and Al_{12.7} alloy at 120 °C (Fig. 8b, c), a maximum decrease of 60 MPa for the transformation stress and a maximum decrease of 0.6% reversible deformation are observed for the cycle C100. The effects of isothermal low cycling fatigue for Al_{10.7} alloy at 240 °C are much more pronounced (Fig. 8d). Only cycle C1 shows a SE with a reversible deformation (ϵ_r) of 2.5% at 240 °C. The irreversible deformation (ϵ_{ir}) increases more rapidly with the number of cycles than for other alloys. At C100, the reversible deformation for Al_{10.7} alloy is limited to 0.5%.

Discussion and Conclusion

Observations of the multicomponent sandwich and SMA ribbon in optical and electron microscopy showed that the bond interface between the CuNiBe master alloy and pure Al is of good quality. The voids in the SMAs ribbons have multiple sources including mechanical and thermal processes, and it is important to limit their number in terms of product quality and durability. To reduce mechanical voids during the co-rolling process, the cleaning steps were reinforced, and a cleaning step was added after the mechanical treatment with the rotary brush. The furnace's atmosphere, time and temperature during the oxidation

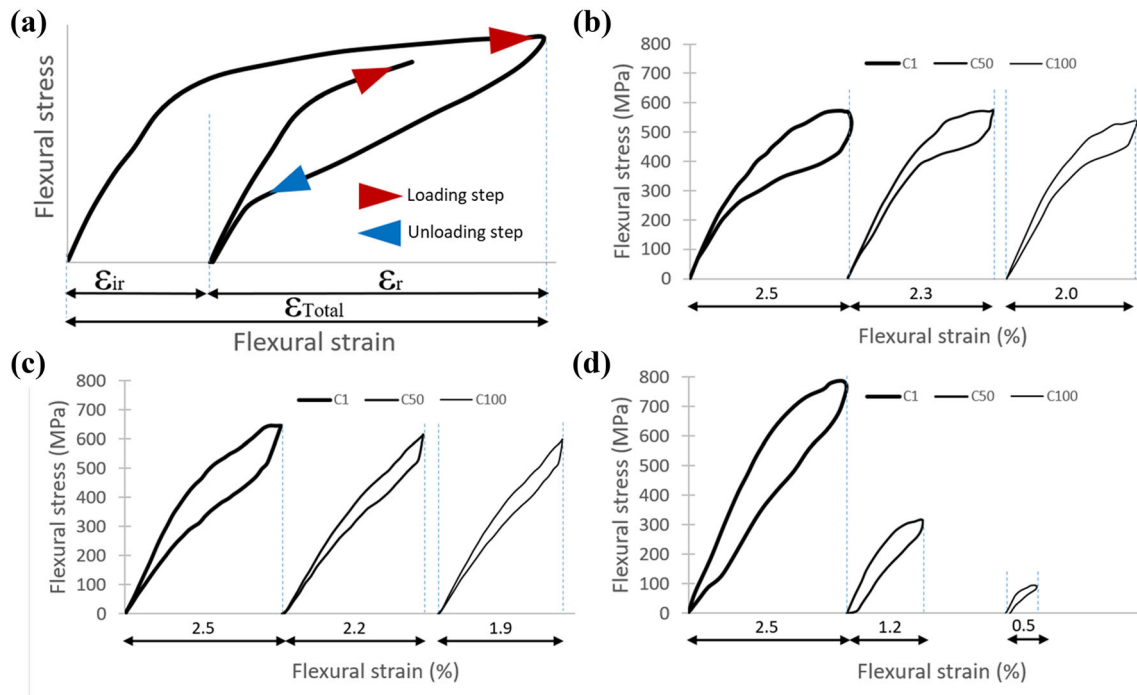


Fig. 8 Three-point bending cycle curves, **a** Explanation of loading/unloading tests, **b** Al_{13.7} alloy at 50 °C, **c** Al_{12.7} alloy at 120 °C, **d** Al_{10.7} alloy at 240 °C

hardening step have been optimized to reduce the number of these holes. To reduce thermal voids during the diffusion steps, each isothermal stage is reached by a heating rate of 2 °C/min. The 670 °C diffusion plateau has also been added to limit the appearance of the voids. The voids present in the final alloy result mainly from the diffusion difference between the elements Al and Cu during the homogenization heat treatment. The transformation temperatures of CuAlNiBe SMAs are very sensitive to variations of Be and Al contents. During SE fatigue cycling, the irrecoverable strain evolves rapidly with the number of thermal cycles for the samples of the Al_{10.7} alloy contrary to the Al_{13.7} and Al_{12.7} samples. From the curves in Fig. 8d, it is evident that the fourth element (beryllium) added to the basic CuAlNi SMA does not allow extended operational suitability at high temperatures (above 200 °C). The tests at 50 °C and 120 °C show that the Al_{13.7} and Al_{12.7} alloys have high serviceability limits. The tests at 240 °C show that the quantities of Be, Al, and Ni elements imposed by the composition of CuNiBe mother alloy do not permit the obtaining of a High Temperature shape memory alloy (HT-SMA). The final thickness of the SMA's ribbons limits naturally the increase in grain size. But the SEM analysis shows too that the number and size of the grains in the section is a function of the initial thicknesses and numbers of the layers in the sandwich (before heat treatment). Thus, small grains are found in the upper and lower layers of the ribbon and larger grains are found in the center of the ribbon. By increasing the number of layers in the sandwiches, the number of grains in the section increases. In this work, the behaviors of these alloys are completely changed due to the variations of the thickness of the Al layer in the primary metallic sandwich. Both alloying elements, Ni and Be, can stabilize beta-phase and restrain the appearance of precipitation phenomena even at high temperatures. CuAlNiBe quaternary alloys are very little studied but the CRB process shows how easy it is to produce this type of alloy with a wide range of different SMAs ribbons both in terms of transformation temperatures, thicknesses, and widths (between 20 and 100 mm). The use of a master alloy makes the CRB process easier to use both in the preparation stages of the strips, in the cold bonding of the metal layers during the first rolling pass as well as in the various diffusion stages.

Acknowledgments This research was supported by the SMART team of the LEM3 laboratory and Nimesis Technology. The authors want to thank sincerely our colleagues Stephane Boulard and Kévin Musseleck, Quentin and Nathan Peltier who provided help that strongly assisted this study.

References

1. Pattor E, Berveiller M (1994) Technologie des Alliages à Mémoire de Forme. Hermès
2. Elmay W, Patoor E, Gloriant T et al (2014) Improvement of superelastic performance of Ti-Nb binary alloys for biomedical applications. *J Mater Eng Perform* 23:2471–2476. <https://doi.org/10.1007/s11665-014-0876-0>
3. Reis R, Gonzalez CH (2008) Fabrication of shape memory alloys using the plasma skull push/pull process. *J Mater Process Technol* 9:3657–3664. <https://doi.org/10.1016/j.jmatprotec.2008.08.025>
4. Vajpai SK, Dube RK, Chatterjee P et al (2012) A novel powder metallurgy processing approach to prepare fine-grained Cu-Al-Ni shape memory alloy strips from elemental powders. *Metall Mater Trans A*. <https://doi.org/10.1007/s11661-012-1081-0>
5. Agrawal A, Dube RK (2018) Methods of fabricating Cu-Al-Ni shape memory alloys. *J Alloys Compd*. <https://doi.org/10.1016/j.jallcom.2018.03.390>
6. Fischer M, Joguelet D, Robin G et al (2016) In situ elaboration of a binary Ti-26Nb alloy by selective laser melting of elemental titanium and niobium mixed powders. *Mater Sci Eng C*. <https://doi.org/10.1016/j.msec.2016.02.033>
7. Fischer M, Laheurte P, Acquier P et al (2017) Synthesis and characterization of Ti-27.5Nb alloy made by CLAD® additive manufacturing process for biomedical applications. *Mater Sci Eng C*. <https://doi.org/10.1016/j.msec.2017.02.060>
8. Lojen G, Anzel I, Kneissl A et al (2005) Microstructure of rapidly solidified Cu–Al–Ni shape memory alloy ribbons. *J Mater Process Technol* 163:220–229. <https://doi.org/10.1016/j.jmatprotec.2005.02.196>
9. Frémond M (1996) Shape memory alloy. In: *Shape Memory Alloys*. International Centre for Mechanical Sciences (Courses and Lectures), vol 351. Springer, Vienna. https://doi.org/10.1007/978-3-7091-4348-3_1
10. Cuniberti A, Montecinos S, Lovey FC (2009) Effect of γ_2 -phase precipitates on the martensitic transformation of a β -CuAlBe shape memory alloy. *Intermetallics* 17:435–440. <https://doi.org/10.1016/j.intermet.2008.12.001>
11. Mukunthan K, Brown LC (1988) Preparation and properties of fine grain β -CuAlNi strain-memory alloys. *Metall Trans A* 19:2921–2929. <https://doi.org/10.1007/BF02647718>
12. Kenji ADACHI, (1989) Formation of X phases and origin of grain refinement effect in Cu-Al-Ni shapememoryalloys added with titanium. *ISIJ Int* 29:378–387
13. Kim JW, Roh DW, Lee ES, Kim YG (1990) Effects on microstructure and tensile properties of a zirconium addition to a Cu-Al-Ni shape memory alloy. *Metall Trans A* 21:741–744. <https://doi.org/10.1007/BF02671945>
14. Vajpai SK, Dube RK, Sangal S (2011) Processing and characterization of Cu-Al-Ni shape memory alloy strips prepared from prealloyed powder by hot densification rolling of powder preforms. *Metall Mater Trans A*. <https://doi.org/10.1007/s11661-011-0728-6>
15. Xu H, Song G, Mao X (2011) Influence of Be and Ni to Cu-Al alloy shape memory performance. *Adv Mater Res* 198:1258–1262. <https://doi.org/10.4028/www.scientific.net/AMR.197-198.1258>
16. Zhu M, Ye X, Li C et al (2009) Preparation of single crystal CuAlNiBe SMA and its performances. *J Alloy Compd* 478:404–410. <https://doi.org/10.1016/j.jallcom.2008.11.051>
17. Recarte V, Pérez-Sáeza R, Bocanegra E et al (1999) Dependence of the martensitic transformation characteristics on concentration in Cu–Al–Ni shape memory alloys. *Mater Sci Eng A* 275:380–384. [https://doi.org/10.1016/S0921-5093\(99\)00302-0](https://doi.org/10.1016/S0921-5093(99)00302-0)

18. Recarte V, Pérez-Sáeza R, Bocanegra E et al (2001) Influence of Al and Ni concentration on the martensitic transformation in Cu-Al-Ni shape-memory alloys. *Metall Mater Trans A*. <https://doi.org/10.1007/s11661-002-0379-8>
19. Delaey N, Mwamba N (1982) The influence on Ni-content on the Ms-temperature OF Cu-Zn-Al-Ni alloys. *J Phys Colloques*. <https://doi.org/10.1051/jphyscol:19824102>
20. Belkahla S, Zufiiga HF, G G, (1993) Elaboration and characterization of new low temperature shape memory Cu-Al-Be alloys. *Mater Sci Eng A* 169:119–124
21. Izadina M, Dehghani K (2011) Structure and properties of nanostructured Cu-13.2Al-5.1Ni shape memory alloy produced by melt spinning. *Trans Nonferrous Met Soc China* 21:2037–2043. [https://doi.org/10.1016/S1003-6326\(11\)60969-2](https://doi.org/10.1016/S1003-6326(11)60969-2)
22. Ergen S, Uzun O, Yilmaz F, Kiliçaslan MF (2013) Shape memory properties and microstructural evolution of rapidly solidified CuAlBe alloys. *Mater Charact* 80:3–8. <https://doi.org/10.1016/j.matchar.2013.03.010>
23. Bay N (1985) Bond strength in cold roll bonding. *Ann CIRP* 34:221–224
24. Bay N (1983) Mechanisms producing metallic bonds in cold welding. *Weld Res Suppl* 62:137–142
25. Jamaati R, Toroghinejad MR (2011) Cold roll bonding bond strengths: review. *Mater Sci Technol* 27:1101–1108. <https://doi.org/10.1179/026708310X12815992418256>
26. Ghalehbandi SM, Malaki M (2019) Accumulative roll bonding—a review. *Appl Sci*. <https://doi.org/10.3390/app9173627>
27. Scarsbrook G (1987) The martensitic transformation behaviour and stabilisation Cu-Zn-Al ribbons. *Acta-Metallurgica* 35:47–56
28. Alizadeh M, Avazzadeh M (2019) Evaluation of Cu-26Zn-5Al shape memory alloy fabricated by accumulative roll bonding process. *Mater Sci Eng A* 757:88–94. <https://doi.org/10.1016/j.msea.2019.04.092>
29. Alizadeh M, Dashtestaninejad MK (2016) Fabrication of manganese-aluminum bronze as a shape memory alloy by accumulative roll bonding process. *JMADE* 111:263–270. <https://doi.org/10.1016/j.matdes.2016.08.074>
30. Moghaddam AO, Ketabchi M, Afrasiabi Y (2014) Accumulative roll bonding and post-deformation annealing of Cu-Al-Mn shape memory alloy. *J Mater Eng Perform* 23:4429–4435. <https://doi.org/10.1007/s11665-014-1228-9>
31. Inoue H, Ishio M, Takasugi T (2003) Texture of TiNi shape memory alloy sheets produced by roll-bonding and solid phase reaction from elementary metals. *Acta Materialia* 51:6373–6383. <https://doi.org/10.1016/j.actamat.2003.08.009>
32. Ye N, Ren X, Liang J (2020) Microstructure and mechanical properties of Ni/Ti/Al/Cu composite produced by accumulative roll bonding (ARB) at room temperature. *Integr Med Res*. <https://doi.org/10.1016/j.jmrt.2020.03.077>
33. Funamizu Y, Watanabe K (1971) Interdiffusion in the Al–Cu System. *Trans Jpn Inst Met* 12(3):147–152. <https://doi.org/10.2320/matertrans1960.12.147>
34. Bowles CQ (1992) Diffusion bonding of beryllium-copper alloys. *J Mater Sc* 27:49–54
35. Schwarz SM, Kempshall BW, Giannuzzi LA (2003) Effects of diffusion induced recrystallization on volume diffusion in the copper-nickel system. *Acta Materialia*. [https://doi.org/10.1016/S1359-6454\(03\)00082-X](https://doi.org/10.1016/S1359-6454(03)00082-X)
36. ASTM F 2004 (2008) Standard test method for transformation temperature of nickel-titanium alloys by thermal analysis
37. ASTM F 2082 (2008) Standard Test Method for Determination of Transformation Temperature of Nickel- Titanium Shape Memory Alloys by Bend and Free Recovery
38. Paul A, Van Dal MJH, Kodentsov AA, Van Loo FJJ (2004) The Kirkendall effect in multiphase diffusion. *Acta Mater* 52:623–630. <https://doi.org/10.1016/j.actamat.2003.10.007>
39. Paul A (2004) The Kirkendall effect in solid state diffusion. *Tech Univ Eindhoven*. <https://doi.org/10.6100/IR579448>
40. De Oliveira DF, de Lima JSG, Brito ICA et al (2010) Mechanical strength evaluation of a CuAlBe shape memory alloy under different thermal conditions. *Mater Sci Forum* 643:105–111. <https://doi.org/10.4028/www.scientific.net/MSF.643.105>
41. Paper O, Soliman HN, Habib N (2014) Effect of ageing treatment on hardness of Cu-12.5 wt% Al shape memory alloy. *Indian J Phys*. <https://doi.org/10.1007/s12648-014-0480-z>
42. Moreau F, Tidu A, Eberhardt A, Heizmann JJ (1995) Study of CuAlBe shape memory alloy by X-ray diffraction. *J Phys IV* 5:1–6
43. Malard B, Sittner P, Berveiller S, Patoor E (2012) Advances in martensitic transformations in Cu-based shape memory alloys achieved by in situ neutron and synchrotron X-ray diffraction methods. *Comptes Rendus Phys* 13:280–292. <https://doi.org/10.1016/j.crhy.2011.12.003>
44. Sharma M, Vajpai SK, Dube RK (2010) Processing and characterization of Cu-Al-Ni shape memory alloy strips prepared from elemental powders via a novel powder metallurgy route. *Metall and Mat Trans A*. <https://doi.org/10.1007/s11661-010-0351-y>
45. Zeifert BH, Salmones J, Cabanas-moreno JG, Calderon HA (2008) Raney-nickel catalysts produced by mechanical alloying. *Rev Adv Mater Sci* 18:633
46. Das N, Dey GK, Murty BS, Pabi SK (2005) On amorphization and nanocomposite formation in Al–Ni–Ti system by mechanical alloying. *Pramana* 65:831–840
47. Cheniti H, Bouabdallah M, Patoor E (2009) High temperature decomposition of the B1 phase in a Cu–Al–Ni shape memory alloy. *J Alloys Compd* 476:420–424. <https://doi.org/10.1016/j.jallcom.2008.09.003>
48. Al-humairi SSN (2019) Cu-based shape memory alloys: modified structures and their related properties. *Recent Adv Metall Eng Electrodepos*. <https://doi.org/10.5772/intechopen.86193>

Publisher’s Note Springer Nature remains neutral with regard to jurisdictional claims in published maps and institutional affiliations.